PHYSICAL REVIEW B **83**, 235313 (2011)

Static conductivity of charged domain walls in uniaxial ferroelectric semiconductors

E. A. Eliseev,[1,2] A. N. Morozovska,[1,*] G. S. Svechnikov,[1] Venkatraman Gopalan,[3] and V. Ya. Shur[4,†]

[1]*Institute of Semiconductor Physics, National Academy of Science of Ukraine, 41, pr. Nauki, UA-03028 Kiev, Ukraine*

[2]*Institute for Problems of Materials Science, National Academy of Science of Ukraine, 3, Krjijanovskogo, UA-03142 Kiev, Ukraine*

[3]*Department of Materials Science and Engineering, Pennsylvania State University, University Park, Pennsylvania 16802, USA*

[4]*Institute of Physics and Applied Mathematics, Ural State University, Ekaterinburg RU-620083, Russia*

(Received 14 March 2011; revised manuscript received 17 April 2011; published 9 June 2011)

By using Landau-Ginzburg-Devonshire theory, we numerically calculated the static conductivity of charged domain walls with different incline angles with respect to the spontaneous polarization vector in the uniaxial ferroelectric semiconductors of n type. We used the effective mass approximation for the electron and hole density of states, which is valid at an arbitrary distance from the domain wall. Due to the electron accumulation, the static conductivity drastically increases at the inclined head-to-head wall by 1 order of magnitude for small incline angles $\theta \sim \pi/40$ and by 3 orders of magnitude for the perpendicular domain wall ($\theta = \pi/2$). There are space-charge regions around the charged domain walls, but the quantitative characteristics of the regions (width and distribution of the carriers) appear very differently for the tail-to-tail and head-to-head walls in the considered donor-doped ferroelectric semiconductor. The head-to-head wall is surrounded by the space-charge layer with accumulated electrons and depleted donors with the same thickness (~40−100 correlation lengths). The tail-to-tail wall is surrounded by the thin space-charge layer with accumulated holes with thicknesses of ~5–10 correlation lengths, a thick layer with accumulated donors with thicknesses of ~100−200 correlation lengths, as well as the layer depleted by electrons with thicknesses of ~100−200 correlation lengths. The conductivity across the tail-to-tail wall is at least an order of magnitude smaller than the one for the head-to-head wall due to the low mobility of the holes, which are improper carriers. The results are in qualitative agreement with recent experimental data for $LiNbO_3$ doped with MgO.

DOI: 10.1103/PhysRevB.83.235313 PACS number(s): 73.40.−c, 77.80.Dj

I. INTRODUCTION

Conductive ferroelectric domain walls are very interesting for fundamental studies as well as promising for nanoelectronics development due to their nanosized width as well as the possibility for controlling their spatial location by external fields. In particular, Seidel *et al.*[1] reported the observation of room-temperature electronic conductivity at ferroelectric domain walls in the insulating multiferroic $BiFeO_3$. The origin of the observed conductivity was probed using a combination of conductive atomic force microscopy, high-resolution transmission electron microscopy, and first-principles density functional computations. Performed analyses revealed that the conductivity distribution correlates with structurally driven changes in both the electrostatic potential and the local electronic structure, which shows a decrease in the band gap at the domain wall.

Charged domain walls cannot be thermodynamically stable in ferroelectrics and ferroelectric semiconductors. However, charged domain walls inevitably originate during the process of ferroelectric polarization reversal. During a real polarization reversal in a ferroelectric capacitor, the needlelike domains with charged domain walls, which arise at the polar surface, move through the sample.[2–5] The formation of the quasiregular-cogged charged domain wall and its expansion have been studied experimentally in $LiNbO_3$ under polarization reversal with uniform metal electrodes.[4] Domain-wall pinning and bowing originate from defect centers.[6] Isolated wedge-shaped domains are formed under the charged scanning probe microscopy probe, which then grow through the uniaxial ferroelectric of nano-, micro-, or millimeter thicknesses acquiring an almost cylindrical shape or a slightly truncated cone[7–10] or long needles.[11–14] Note that, the increase in the conductivity up to 1–3 orders of magnitude along the artificially produced charged domain wall has been measured in a single crystal of the ferroelectric-semiconductor SbSJ.[12]

Charged domain walls, shown in Figs. 1(a)–1(d)**,** depending on the bound charge discontinuity at the wall (i.e., depending on the incline angle θ between the wall plane and the polarization vector of the uniaxial ferroelectric), create strong electric fields, which, in turn, cause free charge accumulation across the wall and sharply increase the domain-wall conductivity. When an inclined domain wall grows through the ferroelectric [as shown in Fig. 1(f)], it may become a conducting channel, and the strong increase in the conductivity current will be registered by current scanning probe microscopy (CSPM), until the wall becomes uncharged again [as shown in Fig. 1(g)]. Since the bound charge distribution is continuous across the uncharged 180° domain wall, such walls do not create any electric fields and naturally do not induce any redistribution of the free charges across the wall.

Analyses of the literature show that the important problem of the charged domain-wall conductivity was not studied enough theoretically. For instance, Guro *et al.*[15,16] used Boltzmann approximation (BA) for the dependence of holes and electrons on the electrostatic potential and consider only perpendicular domain walls, i.e., when the wall plane is perpendicular to the spontaneous polarization vector (for a detailed review, see the textbook of Fridkin[17]). However, the studies consider the intrinsic semiconductor ferroelectrics, while only the oversimplified estimations of the band bending (maximal potential value) and carrier concentrations near the

 ©2011 American Physical Society

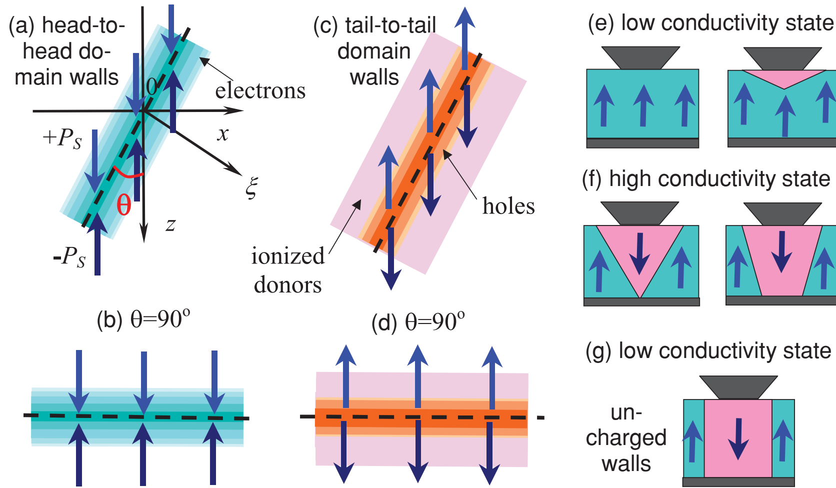

FIG. 1. (Color online) (a)–(d) Sketch of the charged walls in the uniaxial ferroelectric semiconductors of n type: (a) inclined head-to-head, (b) perpendicular head-to-head, (c) inclined tail-to-tail, and perpendicular tail-to-tail domain walls, where the gradient colors indicate the free-carrier concentration [electrons in the case of (a) and (b) and donors + holes in the case of (b) and (d)] increase at the domain-wall vicinity. The incline angle of the domain wall is θ. (e)–(g) When switching from state (e) to state (g), the intermediate high-conductivity state may appear due to the intergrowth of the charged domain walls during the local polarization reversal in the uniaxial ferroelectric semiconductors. External voltage is applied between the CSPM and the bottom electrode.

surface with zero polarization are performed for extrinsic semiconductor ferroelectrics with impurities.

Mokry *et al.*[18] considered an infinitely thin inclined domain wall without any internal structure of the screening and bound charge distribution. Concrete calculations were performed for the case when both bound charges and screening charges (proportional to the bound ones) were localized directly at the domain-wall plane, while the self-consistent calculation of the screening charge distribution across the wall was not performed.

Using Landau theory, Gureev *et al.*[19,20] considered the problem of the structure and energy of a charged 180° head-to-head domain wall. It was found that the scales controlling the wall structure can be very different from the Debye radius. Depending on the spontaneous polarization and the concentration of free carriers, these scales can be about the Thomas-Fermi screening length or about those typical for screening in nonlinear (Thomas-Fermi or Debye) regimes.

To summarize the brief overview, the conductivity distribution across a charged domain wall has not been calculated previously even for uniaxial ferroelectrics. This fact motivates our study: We calculated the static conductivity of both inclined and perpendicular domain walls in the uniaxial ferroelectric semiconductor using the Landau-Ginzburg-Devonshire (LGD) theory. We used the effective-mass approximation for the electron and hole density of states, which is valid at an arbitrary distance from the domain wall.

II. PROBLEM STATEMENT

Let us consider a head-to-head and tail-to-tail inclined wall in a uniaxial ferroelectric semiconductor doped with n-type impurity (e.g., $LiNbO_3$:Fe, Mg, or $LiTaO_3$:Cr, etc.). A sketch of the charged walls is shown in Figs. 1(a)–1(d). The incline angle of the domain wall is regarded as θ. The domain wall is considered infinite and planar. No surface effect is considered. Note that one can ignore the surface influence on the domain-wall properties at distances higher than 10–20 correlation lengths from the ferroelectric surface, i.e., 5–10 nm for $LiNbO_3$ or $LiTaO_3$.

For the uniaxial ferroelectrics, the electric potential $\varphi(x,z)$ and the ferroelectric polarization component $P_z(x,z)$ should be determined from the Poisson equation:

$$\varepsilon_0\left(\varepsilon_{33}^b\frac{\partial^2\varphi}{\partial z^2}+\varepsilon_{11}\frac{\partial^2\varphi}{\partial x^2}\right) = \frac{\partial P_z}{\partial z}-q[N_d^+(\varphi)+p(\varphi)-n(\varphi)-N_a^-], \quad (1a)$$

with boundary conditions of the potential vanishing far from the domain wall.

$$\varphi(r\to\infty)=0,\quad \varphi(r\to-\infty)=0. \quad (1b)$$

The charges are in units of electron charge $q=1.6\times10^{-19}$ C; $\varepsilon_0=8.85\times10^{-12}$ F/m is the universal dielectric constant, ε_{11} is the dielectric permittivity in the direction normal to the polar axis, and ε_{33}^b is the background or base dielectric permittivity different from the ferroelectric soft-mode permittivity ε_{33}.[21–24] For the majority of normal ferroelectrics, $\varepsilon_{33}^b \ll \varepsilon_{33}$, since its origin can be related with electronic polarizability from the nonferroelectric lattice modes of the crystal.[21] Higher values of ε_{33}^b correspond to some incipient ferroelectrics.[25]

Here, ionized deep acceptors with field-independent concentration N_a^- play the role of a background charge; ionized shallow donors, free holes, and electron equilibrium concentration are N_d^+, p, and n. The donor level is regarded to be infinitely thin with activation energy E_d. In this case, the concentration of donors is determined by a single Fermi-Dirac distribution function,[26]

$$N_d^+(\varphi)=N_{d0}[1-f(E_d-E_F-q\varphi)]. \quad (2a)$$

The concentration of the electrons in the conductive band and holes in the valence band is considered in the continuous levels approximation,[27,28]

$$p(\varphi)=\int_0^\infty d\varepsilon g_p(\varepsilon)f(\varepsilon-E_V+E_F+q\varphi) \approx\left(\frac{m_pk_BT}{\hbar^2}\right)^{3/2}\frac{1}{\pi^2\sqrt{2}}\frac{\sqrt{\pi}}{2} \times\left\{-Li_{3/2}\left[-\exp\left(\frac{-q\varphi+E_V-E_F}{k_BT}\right)\right]\right\}, \quad (2b)$$

$$n(\varphi) = \int_0^\infty d\varepsilon g_n(\varepsilon) f(\varepsilon + E_C - E_F - q\varphi) \approx \left(\frac{m_n k_B T}{\hbar^2}\right)^{3/2} \frac{1}{\pi^2\sqrt{2}} \frac{\sqrt{\pi}}{2} \times \left\{-Li_{3/2}\left[-\exp\left(\frac{q\varphi + E_F - E_C}{k_B T}\right)\right]\right\}, \quad (2c)$$

where N_{d0} is the concentration of donor centers, $f(x) = \frac{1}{1+\exp(x/k_B T)}$ is the Fermi-Dirac distribution function, $k_B = 1.3807 \times 10^{-23}$ J/K, T is the absolute temperature, E_F is the Fermi energy level, E_d is the donor level, E_C is the bottom of conductive band, and E_V is the top of the valence band (all energies are counted from the vacuum level). When the bulk density of states is $g_n(\varepsilon) \approx \frac{\sqrt{2m_n^3\varepsilon}}{2\pi^2\hbar^3}$ and $g_p(\varepsilon) \approx \frac{\sqrt{2m_p^3\varepsilon}}{2\pi^2\hbar^3}$ in the effective-mass approximation (usually $m_n \ll m_p$),[26–28,17] one obtains the approximate equalities in Eqs. (2b) and (2c), where $Li_n(z) = \sum_{k=1}^{\infty} \frac{z^k}{k^n}$ is the polylogarithmic function.

Due to the potential vanishing far from the wall [see Eq. (1b)], the condition should be valid,

$$N_a^- = N_{d0}^+ + p_0 - n_0, \quad (3)$$

where $N_{d0}^+ = N_{d0}[1 - f(E_d - E_F)] \equiv N_{d0} f(E_F - E_d)$, $p_0 = \int_0^\infty d\varepsilon g_p(\varepsilon) f(\varepsilon + E_F - F_V)$, and $n_0 = \int_0^\infty d\varepsilon g_n(\varepsilon) f(\varepsilon + E_C - F_F)$.

The polarization distribution satisfies the LGD equation,

$$\alpha(T)P_z + \beta P_z^3 + \gamma P_z^5 - g\left(\frac{\partial^2 P_z}{\partial z^2} + \frac{\partial^2 P_z}{\partial x^2}\right) = -\frac{\partial\varphi}{\partial z}, \quad (4a)$$

with the boundary conditions

$$P_z(r \to \infty) = P_S, \quad P_z(r \to -\infty) = -P_S. \quad (4b)$$

The domain-wall plane is $z/x = -\cot\theta$ [see Fig. 1(a)]. We introduce an another coordinate system, rotated around the y axis on angle θ, and a new variable,

$$\xi = x\cos\theta + z\sin\theta. \quad (5)$$

Far from the crystal plate boundaries, all quantities only depend on ξ, and LGD Eq. (1a) and Poisson Eq. (4a) acquire the form of two coupled equations,

$$\alpha(T)P_z + \beta P_z^3 + \gamma P_z^5 - g\frac{\partial^2 P_z}{\partial \xi^2} = -\sin\theta\frac{\partial\varphi}{\partial\xi}, \quad (6a)$$

$$\varepsilon_0\left(\varepsilon_{33}^b \sin^2\theta + \varepsilon_{11}\cos^2\theta\right)\frac{\partial^2\varphi}{\partial\xi^2} = \sin\theta\frac{\partial P_z}{\partial\xi} - q[N_d^+(\varphi) + p(\varphi) - n(\varphi) - N_a^-], \quad (6b)$$

with boundary conditions from Eqs. (1b) and (4b) written as

$$P_z(\xi \to \infty) = P_S, \quad P_z(\xi \to -\infty) = -P_S, \quad \varphi(\xi \to \infty) = 0, \quad \varphi(\xi \to -\infty) = 0. \quad (6c)$$

Note that the P_x component is nonzero across the wall, since the domain-wall plane is rotated around the y axis and, thus, should have nonzero bond charges, which induce the depolarization field component E_x normal to the domain-wall plane. The field E_x affects both P_z and P_x components, but not P_y, since we suppose that the inclined wall is still parallel to the y axis. Note that the so-called very weak in-plane anisotropy is also present for uniaxial ferroelectrics, such as $LiNbO_3$,[29] but we neglect it and, thus, obtained that $P_y = 0$. Since we consider a uniaxial ferroelectric with transverse dielectric isotropy, we could neglect nonlinearity in the direction normal to the polar axis and suppose that, for P_x and P_y, the ferroelectric is close to the linear dielectric. This immediately leads to the expressions for the polarization components: $P_x(\xi) = \varepsilon_0(\varepsilon_{11} - 1)E_x(\xi) = \varepsilon_0(\varepsilon_{11} - 1)\cos(\theta)E_\perp(\xi)$ and $P_y = \varepsilon_0(\varepsilon_0 - 1)E_y = 0$ and the electric field components $E_z(\xi) = E_\perp(\xi)\sin(\theta)$ and $E_x(\xi) = E_\perp(\xi)\cos(\theta)$, where the field $E_\perp(\xi) = -\frac{\partial\varphi}{\partial\xi}$ is perpendicular to the wall plane so that the coordinate dependence of $P_x(\xi)$ is the same as for $E_\perp(\xi)$.

Donor impact to the static conductivity can be neglected, since the ion mobility (if any) is much smaller than the electron one. So, the static conductivity can be estimated as

$$\sigma(\xi) = q[\eta_e n(\xi) + \eta_p p(\xi)]. \quad (7)$$

It is coordinate dependent as proportional to the charge-carrier concentration. Usually, since $m_n \ll m_p$ (and, therefore, the mobility $\eta_e \gg \eta_p$), the most pronounced is the static electronic conductivity.

III. RESULTS AND DISCUSSION

The numerical solutions for Eqs. (6) are shown in Figs. 2 and 3 for the inclined head-to-head and tail-to-tail domain walls for $LiNbO_3$ material parameters**:** $\varepsilon_{33}^b = 5$, $\varepsilon_{11} = 84$, $\varepsilon_{33} = 30$, $\alpha = -1.95 \times 10^9$ m/F, $\beta = 3.61 \times 10^9$ m^{-5} C^{-2} F^{-1}, $\gamma = 0$, and $g = 3 \times 10^{-10} V^{-1}$ m^{-3} C. The spontaneous polarization is $P_S = \sqrt{-\alpha/\beta} = 0.73$ C/m^2, the coercive field is $E_{\text{coers}} = 2\sqrt{-\alpha^3/27\beta} = 5.5 \times 10^8$ V/m, and the correlation length is $r_c = \sqrt{-g/\alpha} \approx 0.4$ nm. The band gap is 4 eV, the donor level E_d is regarded to be 0.1 eV deep below the conduction band, since an oxygen vacancy and other defects' formation and activation energies in ferroelectrics are about 0.1–2 eV (Refs. 30–36), the effective masses are $m_n = 0.05m_e$ and $m_p = 5m_e$, where m_e is the mass of the free electron, and $N_{d0} = 10^{23}$, 10^{24}, 10^{25}, 10^{26} m^{-3} (without acceptors). Also, we suppose that $\eta_e \approx 100\eta_p$, since $m_n \approx 0.01m_p$.[26] Since the choice for E_d (as well as N_{d0} and the effective masses) depends on the defect or impurity type (and, thus, may vary), we would like to underline that all numerical results presented below remained qualitatively the same in the actual range of the parameter $E_d = 0.1$–1 eV. In particular, the results depend on the effective product $N_{d0}^+ = N_{d0} f(E_F - E_d)$ and the higher the E_d, the more pronounced the carriers accumulation and depletion effect, so we choose the small value $\sim$0.1 eV to obtain the lowest estimation of the static conductivity at the domain wall.

Dependencies of polarization $P_z(\xi)/P_S$, electric field perpendicular to the wall plane $E_\perp(\xi)/E_{\text{coer}}$, potential $\varphi(\xi)$, and concentrations of electrons, ionized donors, and relative static conductivity $\sigma(\xi)/\sigma(\infty)$ on the distance ξ/r_c from the wall plane were calculated for the inclined head-to-head domain wall with different slope angles $\theta = \pi/2, \pi/6, \pi/20, \pi/40, 0$

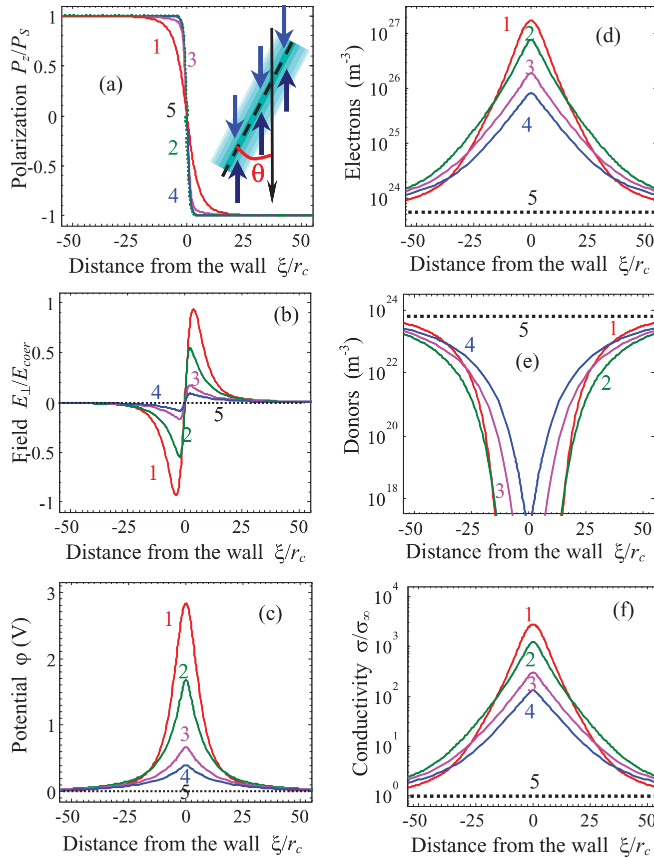

FIG. 2. (Color online) Dependencies of (a) polarization $P_z(\xi)/P_S$, (b) field $E_\perp(\xi)/E_{coer}$, (c) potential $\varphi(\xi)$, (d) concentrations of electrons, (e) ionized donors, and (f) relative static conductivity $\sigma(\xi)/\sigma(\infty)$ calculated for the inclined head-to-head domain wall with different slope angles $\theta = \pi/2, \pi/6, \pi/20, \pi/40, 0$ (curves 1–5) and $N_{d0} = 10^{25}$ m^{-3}. Hole concentration $<10^{-40}$ (i.e., it is absent near the wall). Material parameters correspond to $LiNbO_3$.

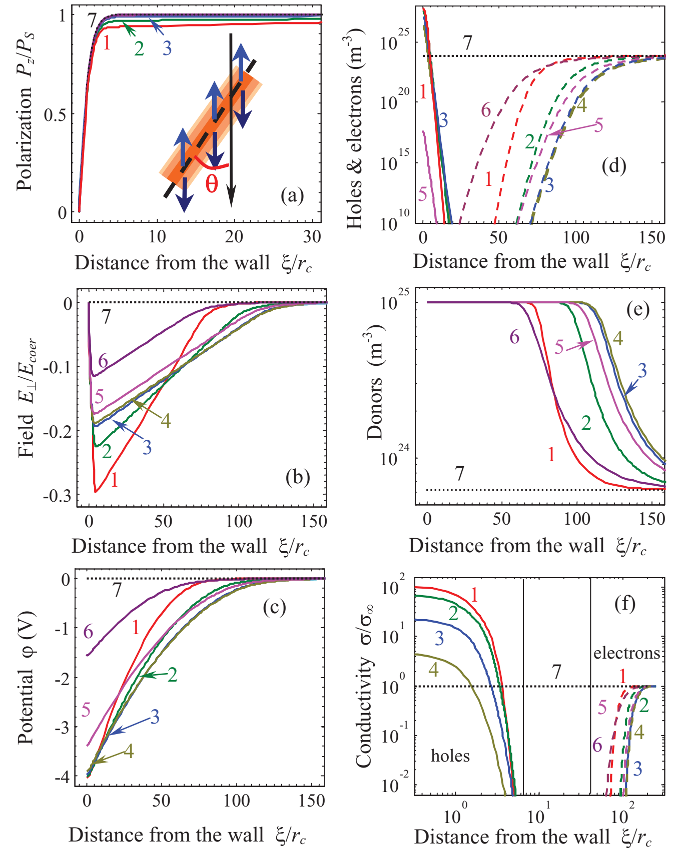

FIG. 3. (Color online) Dependencies of (a) polarization $P_z(\xi)/P_S$, (b) field $E_\perp(\xi)/E_{coer}$, (c) potential $\varphi(\xi)$, (d) concentrations of holes (solid curves) and electrons (dashed curves), (e) ionized donors, and (f) relative static conductivity $\sigma(\xi)/\sigma(\infty)$ calculated for the inclined tail-to-tail domain wall with different slope angles $\theta = \pi/2, \pi/4, \pi/10, \pi/20, \pi/27, \pi/40, 0$ (curves 1–7) and $N_{d0} = 10^{25}$ m^{-3}. Electron concentration $<10^{-40}$ (i.e., it is absent near the wall). Material parameters correspond to $LiNbO_3$.

(see curves 1–5 in Fig. 2). Hole concentration appeared to be less than 10^{-40} m^{-3} (i.e., it is absent near the wall). The uncharged wall is the thinnest; the charged perpendicular wall with maximal bound charge is the thickest [Fig. 2(a)]. Correspondingly, the electric field and potential created by the wall bound charges and screening carriers are the highest for the perpendicular wall ($\theta = \pi/2$) with maximal bound charge $2P_S$; it decreases with the bound charge decrease, i.e., with θ decrease, since the bound charge is $2P_S \sin\theta$, and naturally vanishes at $\theta = 0$ [Figs. 2(b) and 2(c)]. The net electric field of the bound charge attracts free electrons [see accumulation region $|\xi| < 25r_c$ in Fig. 2(d)] and repulses ionized donors [see depletion region $|\xi| < 25r_c$ in Fig. 1(e)] from the charged wall region. The electron concentration is the highest for the perpendicular wall ($\theta = \pi/2$); it decreases with the bound charge decrease (i.e., with θ decrease) and vanishes at $\theta = 0$ [compare maximal values for different curves in Fig. 2(d)]. As a result of electron accumulation, the static conductivity drastically increases at the wall, from 3 orders of magnitude for $\theta = \pi/2$ to 1 order of magnitude for $\theta = \pi/40$ [Fig. 2(e)]. Donor impact on the static conductivity of the head-to-head domain walls can be neglected, since ion mobility (if any) is much smaller than the electron one.

By analyzing the results shown in Figs. 2(c)–(e), one could lead to the following conclusions about the applicability of the most commonly used approximations for the charge-carrier concentration across the charged head-to-head domain wall:

(1) Debye approximation in Eqs. (2) that demands $|q\varphi| \ll k_BT$ becomes valid only very far ($|\xi| \gg 25r_c$) from the charged domain wall in $LiNbO_3$, since $|q\varphi| < k_BT$ only at $|\xi| \gg 25r_c$ even for $\theta = \pi/40$ [see Fig. 2(c), and use $k_BT = 0.025$ eV at room temperature].

(2) BA for electrons, $n(\varphi) \approx n_0 \exp(q\varphi/k_BT)$, is invalid in the immediate vicinity of charged domain walls ($|\xi| < 10r_c$) allowing for their strong accumulation here. Approximation of a strongly degenerate electron gas (DEG), $(\varphi) \approx \frac{(2m_n)^{3/2}}{3\pi^2\hbar^3}(q\varphi + E_F - E_C)^{3/2}$, is valid in the immediate vicinity of the domain walls. BA for holes, $p(\varphi) \approx p_0 \exp(-q\varphi/k_BT)$, is valid everywhere. BA for donors, $N_d^+(\varphi) \approx N_{d0}^+ \exp(-q\varphi/k_BT)$, is valid in the vicinity of the domain wall ($|\xi| < 25r_c$) [see Figs. 2(c) and 2(d)].

Dependencies of polarization, electric field, potential, concentrations of holes, electrons, ionized donors, and relative static conductivity on the distance ξ/r_c from the wall plane was

calculated for the inclined tail-to-tail domain wall with different slope angles $\theta = \pi/2, \pi/4, \pi/10, \pi/20, \pi/27, \pi/40, 0$ (see curves 1–7 in Fig. 3). Note that only half of the tail-to-tail domain wall is shown in Fig. 3 for the sake of clarity. Polarization of the uncharged wall saturates most quickly; the charged perpendicular wall with maximal bound charge saturates most slowly, but the difference is small [compare different curves in Fig. 3(a)]. Electric field and potential created by the wall bound charges and screening carriers are the highest for the perpendicular wall ($\theta = \pi/2$) with maximal bound $2P_S$; it decreases with the bound charge decrease, i.e., with θ decrease, since the bound charge is $2P_S \sin\theta$, and naturally vanishes at $\theta = 0$ [Figs 3(b) and 3(c)]. The net electric field of the bound charge attracts holes in a very thin accumulation region $|\xi| < 5r_c$ [see solid curves in Figs. 3(d) and 3(f)] and ionized donors [see thick depletion region $|\xi| < 100r_c$ in Fig. 3(e)] and repulses electrons from the charged wall region [see dashed curves in Figs. 3(d) and 3(f)]. The hole concentration is the highest for the perpendicular wall ($\theta = \pi/2$); it decreases with the bound charge decrease (i.e., with θ decrease) and vanishes at $\theta = 0$ [compare maximal values for different curves in Fig. 3(d)]. Electron concentration appeared to be less than 10^{-40} m^{-3} near the wall but dominates far from the wall as anticipated for the n-type semiconductor [see dashed curves in Fig. 3(d)]. As a result of hole accumulation, the static conductivity drastically increases at the wall, to 2 orders of magnitude [Fig. 3(f)]. Despite the qualitative similarity, the situation for the conductivity across the tail-to-tail wall is quantitatively different from the one for the head-to-head wall: We see a very thin accumulation region of mobile holes near the tail-to-tail wall and a very thick region of almost immobile donors that does not contribute to the wall conductivity, while the accumulation of mobile electrons is much thicker for the head-to-head wall [compare Figs. 2(f) and 3(f)].

By analyzing the results shown in Figs. 3(c)–3(e), one could lead to the conclusion about the applicability of the most commonly used approximations for the charge-carrier concentration across the charged tail-to-tail domain wall:

(1) Debye approximation in Eqs. (2) that demands $|q\varphi| \ll k_B T$ becomes valid only very far ($|\xi| \gg 25r_c$) from the charged domain wall in $LiNbO_3$, since $|q\varphi| < k_B T$ only at $|\xi| \gg 25r_c$ even for $\theta = \pi/40$ [see Fig. 3(c)].

(2) BA for holes, $p(\varphi) \approx p_0 \exp(-q\varphi/k_B T)$, is invalid in the immediate vicinity of charged domain walls ($|\xi| < 10r_c$), allowing for their strong accumulation here. Approximation of a strong DEG, $p(\varphi) \approx \frac{(2m_n)^{3/2}}{3\pi^2\hbar^3}(-q\varphi - E_F + E_V)^{3/2}$, is valid in the immediate vicinity of the domain walls. BA for electrons, $n(\varphi) \approx n_0 \exp(+q\varphi/k_B T)$, is valid near the wall. Full ionization of donors, $N_d^+(\varphi) \approx N_{d0}$, is valid in the vicinity of the domain wall ($|\xi| < 25r_c$) [see Figs. 3(c) and 3(d)].

Dependencies of polarization, electric field, potential, concentrations of electrons, holes, ionized donors, and relative static conductivity vs distance ξ/r_c from the wall plane was calculated for the limiting case of the perpendicular domain walls (see Figs. 4 and 5).

It can be seen from Figs. 4(a)–4(c), calculated for the head-to-head wall, that profiles of polarization, potential, and electric field across the wall are practically independent of N_{d0}^+, since the screening is dominated by electrons [Fig. 4(d)] and the donor level is filled [concentration of ionized donors is small, see Fig. 4(e)] near the head-to-head wall (holes are absent everywhere). As a result of electron accumulation, the static conductivity drastically increases at the wall [see Fig. 4(f)].

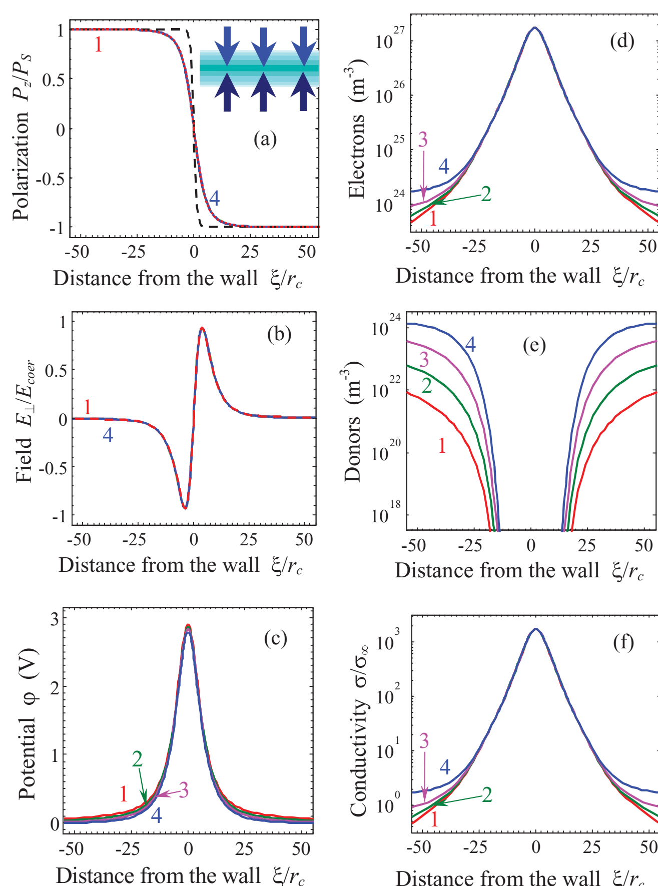

FIG. 4. (Color online) Dependencies of (a) polarization $P_z(\xi)/P_S$, (b) field $E_\perp(\xi)/E_{coer}$, (c) potential $\varphi(\xi)$, and concentrations of (d) electrons, (e) ionized donors, and (f) relative static conductivity $\sigma(\xi)/\sigma(\infty)$ calculated for the perpendicular head-to-head domain wall ($\theta = \pi/2$) and different $N_{d0} = 10^{23}$, 10^{24}, 10^{25}, 10^{26} m^{-3} (curves 1–4). The dashed curve in (a) is the profile of the 180° uncharged domain wall. Hole concentration $<10^{-40}$ (i.e., it is absent near the wall). Material parameters correspond to $LiNbO_3$.

In contrast to the head-to-head walls, the profiles of polarization, potential, and electric field across the perpendicular tail-to-tail domain walls essentially depends on donor concentration N_{d0}^+, since here, the negative bound charges are accumulated at the wall, which have to be screened by holes and ionized donors [see Figs. 5(a)–5(c)]. Note that only half of the tail-to-tail domain wall is shown in Fig. 5 for the sake of clarity. Since the equilibrium concentration of holes (improper carriers) is very small for the considered donor-type ferroelectric in comparison with the electrons, it should be enhanced near the tail-to-tail wall by either direct transition of electrons through the band gap or by donor ionization. However, the hole concentration increase is very limited by

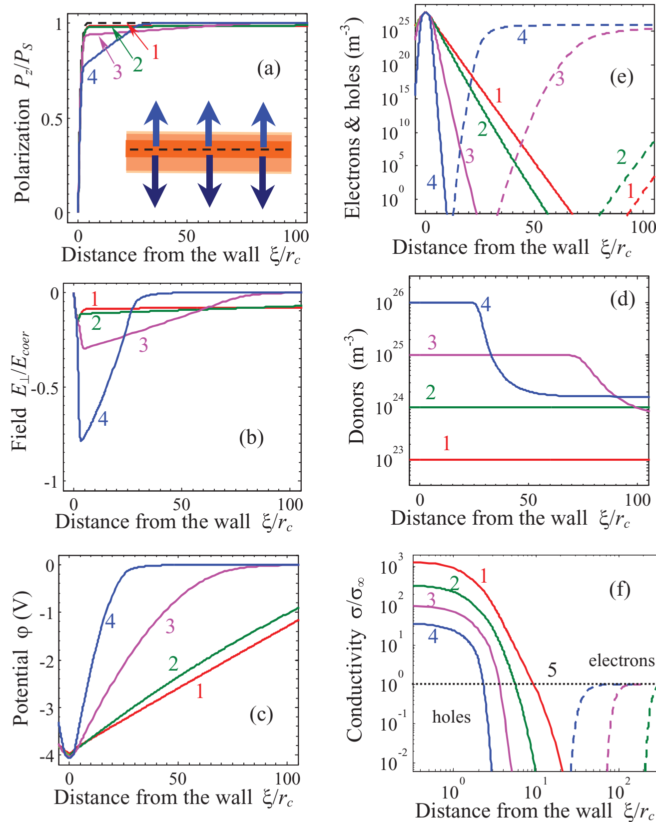

FIG. 5. (Color online) Dependencies of (a) polarization $P_z(\xi)/P_S$, (b) field $E_\perp(\xi)/E_{coer}$, (c) potential $\varphi(\xi)$, concentrations of (d) electrons (dashed curves) and holes (solid curves), (e) ionized donors, and (f) relative static conductivity $\sigma(\xi)/\sigma(\infty)$ for a perpendicular tail-to-tail domain wall ($\theta = \pi/2$) calculated for different $N_{d0} = 10^{23}$, 10^{24}, 10^{25}, 10^{26} m^{-3} (curves 1–4). The dashed curve in (a) is the profile of the 180° domain wall (uncharged). Material parameters correspond to $LiNbO_3$.

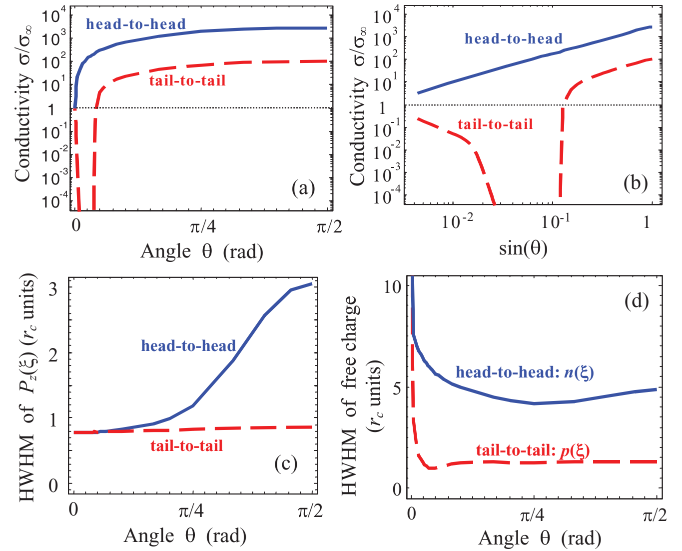

FIG. 6. (Color online) Dependence of the static conductivity at the domain-wall plane $\xi = 0$ [(a) log-linear scale, (b) log-log scale], HWHM of (c) the polarization profile and (d) the mobile screening charges on the wall incline angle θ for head-to-head (solid curves) and tail-to-tail domain walls (dashed curves). Immobile ionized donors θ—dependence is shown by the dotted curve.

the donor ionization, and as a result, the structure of the perpendicular tail-to-tail wall is completely different from the structure of the head-to-head one [compare Fig. 5(a) with Fig. 4(a)]. Actually, one can see two separate regions of the space-charge accumulation: the thin region in the immediate vicinity of the perpendicular wall with accumulated holes and the much wider region with ionized donors [Figs. 5(d)–5(f)].

Dependence of the static conductivity at the domain-wall plane $\xi = 0$, half width at half maximum (HWHM) of the polarization profile, and mobile screening charges (electrons and holes) on the wall incline angle θ are compared in Fig. 6 for head-to-head and tail-to tail domain walls.

From Figs. 6(a) and 6(b), it can be seen that the static conductivity of the head-to-head wall is much higher ($\sim$30 times) than the one of the tail-to-tail wall for the considered n-type semiconductor ferroelectric. Actually, the bound charge $+2P_S \sin\theta$ of the head-to-head wall is screened by the majority carriers—electrons, whose mobility and average concentration are much higher than for the minority carriers—heavy holes, which screen the bound charge $-2P_S \sin\theta$ of the tail-to-tail wall. From Fig. 6(b), it can be seen (plotted in double logarithmic scale) that the conductivity of the head-to head wall is linearly proportional to $\sin\theta$. The conductivity of the tail-to tail wall is linearly proportional to $\sin\theta$ except in the region of small $\sin\theta < 0.1$, where a dip unexpectedly appears. The dip originated from the fact that the amount of holes drastically decreases in the region $0.01 < \sin\theta < 0.1$, and almost immobile ionized acceptors performed the screening of the bound charge $-2P_S \sin\theta$.

From Fig. 6(c), it can be seen that the half width of the polarization profile of the head-to-head wall is only slightly higher (from 1–1.5 times at $\theta < \pi/4$ to 3 times at $\theta \to \pi/2$) than the one of the tail-to-tail wall. The half width of the screening electrons distribution across the head-to-head wall is always several times higher than the half width of the screening hole distribution across the tail-to-tail wall, except the limit of the uncharged wall $\theta \to 0$ [see Fig. 6(d)]. The half width of the screening charge nonmonotonically depends on the wall incline angle θ . At very small angles ($\sin\theta \ll 0.1$), the wall bound charge becomes rather small, and the screening carrier accumulation diffuses and becomes faint; as a result, the half width drastically increases. With θ increase, the plateau (for the tail-to-tail wall) or very broad minimum (for the head-to-head wall) appears at $\theta \sim \pi/4$. With further θ increase from $\pi/4$ to $\pi/2$, the half width of the head-to-head wall slightly increases.

To summarize, the structure of the screening charge distribution and static conductivity across the charged inclined head-to-head and tail-to-tail domain walls are very different in the n-type semiconductor ferroelectrics.

(1) Mobile electrons are accumulated in the vicinity of the head-to-head wall, which screen its bound charge $+2P_S \sin\theta$. The electric field and potential created by the wall bound charges and screening electrons (proper carriers) are the highest for the perpendicular wall (incline angle $\theta = \pi/2$) with maximal bound $2P_S$; it decreases with the bound charge decrease, i.e., with θ decrease, since the bound charge is $2P_S \sin\theta$, and naturally vanishes at $\theta = 0$. As a result

of electron accumulation, the static conductivity drastically increases at the wall, from 3 orders of magnitude for $\theta = \pi/2$ to 1 order of magnitude for $\theta = \pi/40$.

(2) There are space-charge regions around the charged domain walls, but the quantitative characteristics of the regions (width, type of the carriers, and their distribution) appeared to be very different for the tail-to-tail and head-to-head walls in the considered donor-doped ferroelectric semiconductor $LiNbO_3$. In particular, the head-to-head wall is surrounded by the space-charge layer with accumulated electrons and depleted donors with thicknesses of ∼40–100 correlation lengths [see Figs. 2(d) and 2(e)]. For this case, the thicknesses of both layers almost coincide. The tail-to-tail wall is surrounded by the space-charge layer with accumulated holes with thicknesses of ∼5–10 correlation lengths and accumulated donors with thicknesses of ∼60–200 correlation lengths; the layer depleted by electrons has a thickness of ∼100–200 correlation lengths [see Figs. 3(d) and 3(e)]. So, in contrast to the head-to-head walls with almost coinciding depleted and accumulated layers of opposite space charges, the layers have different thicknesses for the tail-to-tail walls in the considered donor-doped ferroelectric semiconductor. Namely, separated regions of the space-charge accumulation exist across a tail-to-tail wall, the thin region in the immediate vicinity of the wall with accumulated mobile holes and depleted of electrons, and the much wider region with ionized donors. We expect that the situation should be vise versa in the acceptor-doped ferroelectric semiconductors.

(3) Donor impact to the static conductivity of the domain walls can be neglected, since ion mobility (if any) is much smaller than the electron one. The conductivity across the tail-to-tail wall is, at least, an order of magnitude smaller than the one for the head-to-head wall due to the low mobility of the holes, which are improper carriers.

(4) Numerical results are compared with the model BA for electrons and the degenerated gas one. We have shown that BA is valid far from the charged wall plane, while the degenerated gas one is valid specifically at the wall plane.

(5) The high-conductivity state may appear due to the intergrowth of the charged domain walls during the local polarization reversal in uniaxial ferroelectrics semiconductors [Fig. 1(d)]. The result is in qualitative agreement with recent experimental data for $LiNbO_3$ doped with MgO.[37]

ACKNOWLEDGMENTS

A.N.M. and E.A.E. gratefully acknowledge multiple discussions with Sergei V. Kalinin (ORNL). E.A.E., A.N.M., and G.S.V. acknowledge the financial support of the NAS Ukraine and Ukraine State Agency on Science, Innovation and Informatization (UU30/004). Research was sponsored, in part, by (V.G., G.S.V., E.A.E., and A.N.M.) the National Science Foundation (Grants No. DMR-0908718 and No. DMR-0820404). E.A.E., A.N.M., and G.S.V. acknowledge user agreement with CNMS N UR-08-869.

APPENDIX

1. BA approximation

In the BA, the Fermi-Dirac distribution function can be approximated as $f(x) \approx \exp(-x/k_BT)$, and the concentrations (2) acquire the form

$$N_d^+(\varphi) \approx N_{d0}^+ \exp\left(\frac{-q\varphi}{k_BT}\right), \quad p(\varphi) \approx p_0 \exp\left(\frac{-q\varphi}{k_BT}\right),$$
$$n(\varphi) \approx n_0 \exp\left(\frac{q\varphi}{k_BT}\right). \tag{A1}$$

2. DEG approximation

For a strong DEG, the Fermi-Dirac distribution function can be approximated by a step function, $f(x) \approx \theta(x/k_BT)$, and the concentrations (2) acquire the form

$$N_d^+(\varphi) = \frac{N_{d0}}{1 + \exp\left(-\frac{E_d - E_F - q\varphi}{k_BT}\right)}, \tag{A2a}$$

$$p(\varphi) \approx \frac{(2m_p)^{3/2}}{3\pi^2\hbar^3}(-q\varphi + E_V - E_F)^{3/2},$$
$$n(\varphi) \approx \frac{(2m_n)^{3/2}}{3\pi^2\hbar^3}(q\varphi + E_F - E_C)^{3/2}, \tag{A2b}$$

*morozo@i.com.ua
†vladimir.shur@usu.ru

[1] J. Seidel, L. W. Martin, Q. He, Q. Zhan, Y.-H. Chu, A. Rother, M. E. Hawkridge, P. Maksymovych, P. Yu, M. Gajek, N. Balke, S. V. Kalinin, S. Gemming, F. Wang, G. Catalan, J. F. Scott, N. A. Spaldin, J. Orenstein, and R. Ramesh, Nature Mater. **8**, 229 (2009).
[2] V. Ya. Shur, in *Nucleation Theory and Applications*, edited by J. W. P. Schmelzer (Wiley –VCH, Weinheim, 2005), Ch. 6, pp. 178–214.
[3] V. Ya. Shur, Ferroelectrics **340**, 3 (2006).
[4] V. Ya. Shur, E. L. Rumyantsev, E. V. Nikolaeva, and E. I. Shishkin, Appl. Phys. Lett. **77**, 3636 (2000).
[5] P. S. Zelenovskiy, V. Ya. Shur, P. Bourson, M. D. Fontana, D. K. Kuznetsov, and E. A. Mingaliev, Ferroelectrics **398**, 34 (2010).
[6] T. J. Yang, V. Gopalan, P. J. Swart, and U. Mohideen, Phys. Rev. Lett. **82**, 4106 (1999).
[7] K. Fujimoto and Y. Cho, Appl. Phys. Lett. **83**, 5265 (2003).
[8] D. Xue, S. Wu, Y. Zhu, K. Terabe, K. Kitamura, and J. Wang, Chem. Phys. Lett. **377**, 475 (2003).
[9] Y. Cho, S. Hashimoto, N. Odagawa, K. Tanaka, and Y. Hiranaga, Nanotechnology **17**, S137 (2006).
[10] Y. Cho, S. Hashimoto, N. Odagawa, K. Tanaka, and Y. Hiranaga, Appl. Phys. Lett. **87**, 232907 (2005).
[11] M. Molotskii, A. Agronin, P. Urenski, M. Shvebelman, G. Rosenman, and Y. Rosenwaks, Phys. Rev. Lett. **90**, 107601 (2003).
[12] A. A. Grekov, A. A. Adonin, and N. P. Protsenko, Ferroelectrics **12**, 483 (1975).
[13] A. Agronin, M. Molotskii, Y. Rosenwaks, G. Rosenman, B. J. Rodriguez, A. I. Kingon, and A. Gruverman, J. Appl. Phys. **99**, 104102 (2006).
[14] V. Gopalan and T. E. Mitchell, J. Appl. Phys. **83**, 941 (1998).

[15]G. M. Guro, I. I. Ivanchik, and N. F. Kovtonuk, Fiz. Tverd. Tela (Leningrad) **10**, 134 (1968) [Sov. Phys. Solid State **10**, 100 (1968)].
[16]G. I. Guro, I. I. Ivanchik, and N. F. Kovtoniuk, Fiz. Tverd. Tela (Leningrad) **11**, 1956 (1969) [Sov. Phys. Solid State **11**, 1574 (1970)].
[17]V. M. Fridkin, *Ferroelectrics Semiconductors* (Consultant Bureau, New-York and London, 1980).
[18]P. Mokry, A. K. Tagantsev, and J. Fousek, Phys. Rev. B **75**, 094110 (2007).
[19]M. Y. Gureev, A. K. Tagantsev, and N. Setter, in *18th IEEE International Symposium on the Applications of Ferroelectrics, 2009, ISAF 2009* (IEEE, Piscataway, NJ, 2009).
[20]M. Y. Gureev, A. K. Tagantsev, and N. Setter, Phys. Rev. B **83**, 184104 (2011).
[21]A. K. Tagantsev and G. Gerra, J. Appl. Phys. **100**, 051607 (2006).
[22]C. H. Woo and Yue Zheng, Appl. Phys. A: Mater. Sci. Process. **91**, 59 (2007).
[23]A. M. Bratkovsky and A. P. Levanyuk, e-print arXiv:0801.1669.
[24]G. Rupprecht and R. O. Bell, Phys. Rev. **135**, A748 (1964).
[25]T. Katsufuji and H. Takagi, Phys. Rev. B **64**, 054415 (2001).
[26]N. W. Ashcroft and N. D. Mermin, *Solid State Physics* (Holt, Rinehart and Winston, New York, 1976).
[27]S. M. Sze, *Physics of Semiconductor Devices*, 2nd ed. (Wiley-Interscience, New York, 1981).
[28]A. I. Anselm, *Introduction to Semiconductor Theory* (Mir, Moscow/Prentice-Hall, Englewood Cliffs, NJ, 1981).
[29]D. A. Scrymgeour, V. Gopalan, Amit Itagi, Avadh Saxena, and P. J. Swart, Phys. Rev. B **71**, 184110 (2005).
[30]M. DiDomenico Jr., and S. H. Wemple, Phys. Rev. **155**, 539 (1967).
[31]R. Moos, W. Mcnesklou, and K. H. Hardtl, Appl. Phys. A: Mater. Sci. Process. **61**, 389 (1995).
[32]Ralf Moos and Karl Heinz Härdtl, J. Appl. Phys. **80**, 393 (1996).
[33]G. A. Gamal, M. M. Abdalrahman, M. I. Ashraf, and H. J. Eman, J. Phys. Chem. Solids **66**, 1 (2005).
[34]Haixuan Xu, Donghwa Lee, Jun He, Susan B. Sinnott, Venkatraman Gopalan, Volkmar Dierolf, and Simon R. Phillpot, Phys. Rev. B **78**, 174103 (2008).
[35]Haixuan Xu, Donghwa Lee, Susan B. Sinnott, Venkatraman Gopalan, Volkmar Dierolf, and Simon R. Phillpot, Phys. Rev. B **80**, 144104 (2009).
[36]Haixuan Xu, Aleksandr Chernatynskiy, Donghwa Lee, Susan B. Sinnott, Venkatraman Gopalan, Volkmar Dierolf, and Simon R. Phillpot, Phys. Rev. B **82**, 184109 (2010).
[37]V. Ya. Shur, A. V. Ievlev, E. V. Nikolaeva, E. I. Shishkin, and M. M. Neradovskiy (unpublished).